Trends in Cell & Molecular Biology
Vol. 9, 2014

Original Communication

Regulation of the frequency and wavelength of calcium waves propagating in networks of interconnected cells: A simulation study

Juexuan Long[1,*], Pierre A. Deymier[1], Keith Runge[1] and James B. Hoying[2]

[1]Department of Materials Science and Engineering, University of Arizona, Tucson AZ 85721, USA;
[2]Cardiovascular Innovation Institute, University of Louisville/Jewish Heritage Foundation, 302 E Muhammad Ali Blvd., Louisville, KY 40202, USA.

ABSTRACT

We develop a model-based theoretical framework to shed light on the phenomenon of cross-level interactions in complex and dynamic multicellular structures with a focus on calcium signaling via calcium waves. In particular, we investigate computationally the interdependence between intracellular calcium and inositol-1,4,5-trisphosphate (IP_3) pathway and cell-cell communication via gap junction intercellular diffusion of Ca^{2+} and IP_3. To enable the propagation of calcium waves in a one-dimensional chain of cells, we introduce a calcium concentration-dependent threshold-based mechanism to trigger calcium oscillations of individual cells. Our model shows that the dynamics of cells embedded in a multicellular network is significantly different from that of an isolated cell. In particular, we have demonstrated that the transient and steady state frequency of calcium oscillations of a cell stimulated with an agonist depends on its microenvironment, in this case, its cell neighbors. The neighborhood of the stimulated cell forms a "signaling niche" that acts on the stimulated cell itself and dynamically regulates its oscillation frequency. This effect is attributed to a crosstalk between the stimulated cell and its environment through retrograde diffusion of calcium and IP_3.

KEYWORDS: wave-trains, multicellular, oscillation frequency, microenvironment

*Corresponding author: juexuanl@email.arizona.edu

INTRODUCTION

Multi-level organization and dynamics is a hallmark feature of most biological systems. This is particularly true in cellular tissues in which single cells are organized into complex multi-cellular tissues. Central to the proper behavior in these biological systems is cross-level interdependence. To date, studies of signaling in multicellular networks have demonstrated that the architecture of these networks can have a significant impact on the behavior of individual cells as well as their emerging collective behavior. For instance, there is strong evidence that the branching architecture of the mammary gland and associated cellular signaling determine epithelial cell function [1, 2] or dysregulation [3]. Additionally, faulty cellular organization can facilitate the cell transformations leading to further neoplasia and cancer [4, 5]. Conversely, normal cellular architecture can suppress tumor formation and prevent malignant phenotypes even in grossly abnormal cells [6]. Furthermore, it has become increasingly clear that effective tissue engineering strategies require constructed cell systems to be appropriately organized in order to support the proper intercellular behavior for a desired tissue function [7-9].

A particular aspect of cellular networks is the interacting behavior of the cells beyond a simple summation of individual element activities. With respect to cellular networks, the passing of signals between cells of the network is one way in which new system behaviors can emerge. For instance, intercellular calcium waves were observed

to define communication networks among neural progenitor cells [10]. Also astrocytes of the cortical gray matter appear to play an active role in brain function that takes the form of calcium waves that propagate between cells within networks of astrocytes [11]. Central to understanding these emergent processes is that cellular networks inherently combine dynamical and structural complexity, making it difficult to isolate single cell versus emergent network behavior. However, the relationships between network dynamics and architecture have been successfully investigated using a variety of physical and mathematical approaches [12], many of which have been applied to understand the complexities of neuronal circuitry. For example, embryonic stem cell-derived neural progenitors form networks exhibiting synchronous calcium signaling activity. This coherent calcium dynamic was shown to be correlated across so called small-world networks [13]; networks with the mean shortest distance between nodes scaled logarithmically with the number of nodes.

The objective of the present study is to develop a model-based theoretical framework to shed light on the phenomenon of cross-level interactions in complex and dynamic multicellular structures with a focus on calcium signaling via calcium waves. Calcium signaling occurs in nearly all cell types and calcium waves are a common phenomenon in multicellular systems. In particular, we are interested in the interplay between intracellular calcium activity and intercellular propagation in networks of cells. From a theoretical perspective, Othmer and Scriven [14] developed, following Turing's pioneering mathematical treatise of morphogenesis [15], an analysis technique in which the information about the underlying network topology, through a connectivity matrix, is decoupled from that of the intracellular reaction pathway mechanism, thus enabling progress in multicellular network research that includes complexity at both low and high levels. In a previous series of studies [16, 17], we reported the use of Green's function-based Interface Response Theory (IRT) [18], a method originally developed for tackling composite media in condensed matter physics, to augment Scriven-Othmer's method to solve coupled dynamical networks with nontrivial connectivity matrices and therefore integrate natural biological organization from the cellular level to complex network architectures. Because simple vascular endothelial cell networks are capable of both downstream and upstream signal conduction between interconnected endothelial cells [19], they can be used as an example of biological context to calculate the spectrum of propagating linear compositional waves in models of multicellular architectures and study putative signal conduction dynamics across networks of endothelial cell models [20]. We also conducted an experimental and computational study of calcium wave propagation in chains of model cells with nonlinear intracellular calcium dynamics and showed the importance of local cell environment on the transmission of a pulse through junctions in multicellular networks [21]. For the sake of mathematical tractability, we assumed in that model an effective nonlinear intracellular reaction dynamic involving only Ca^{2+}. For this we utilized a simple piecewise-linear model of the nonlinear Ca^{2+} intracellular reaction dynamics. This modeled the Ca^{2+} depletion of the cytoplasm and repletion separated by a threshold concentration. Many have used different mathematical models to better understand propagation dynamics, including addressing gap junction-dependent processes [22, 23]. A nonlinear model of the gap junctional mechanisms was developed to demonstrate long-range propagation of intercellular Ca^{2+} waves in networks of astrocytes [24]. While not gap junction-specific, others have modeled intra- and extra-cellular calcium dynamics based on ICC (Intercellular Calcium Communication) [25, 26] and CICR (Calcium Induced Calcium Release) models [27-29]. In many cell types, extracellular stimuli can be converted into intracellular signals in the form of Ca^{2+} oscillations. These intracellular oscillations depend on the dose of the applied extracellular agonist [30]. Politi *et al.* introduced a model that can simulate the increase of the frequency of intracellular calcium oscillation with stepwise increases in the agonist concentration [31].

In this paper we develop a model of calcium wave propagation in a chain of cells incorporating both intracellular calcium dynamics and intercellular calcium wave propagation. We investigate computationally the effect of cross-level interdependence between intracellular calcium-IP_3 pathway and cell-cell communication via intercellular diffusion of both Ca^{2+} and IP_3. In contrast to Goldberg's model [24], diffusion in our model is linear with a diffusion coefficient that is independent of Ca^{2+}/IP_3 concentration. However, to achieve

long-distance intercellular calcium wave propagation a regeneration mechanism of IP_3 is evoked. This mechanism depends on the cytosolic Ca^{2+} concentration. We investigate the effect of the chain-like architecture of the multicellular network on the frequency of calcium oscillations of individual cells and the wavelength of trains of calcium waves. Significant cross-level effects are found on the transient behavior of individual cells as well as their steady oscillatory state. We show that the intracellular oscillation frequency of an individual cell embedded in the chain-like network and stimulated with an agonist differs at steady state from that of an isolated cell. Furthermore, the transient behavior of that stimulated cell toward steady oscillations is taking significantly longer in the multicellular network. In fact, the stimulated cell generates sequential trains of pulses with increasing frequency. These trains of pulses are supported and propagating along the chain of cells. The mechanism for this long time transient behavior is attributed to retrograde diffusion of calcium and IP_3 originating from a widening range of cells in the chain undergoing oscillations as the trains of pulses propagate. This mechanism highlights the importance of microenvironment on the dynamical behavior of cells in multicellular networks. In particular, this study demonstrates that the dynamical behavior of a specific cell embedded in a multicellular environment depends on crosstalk between the cell and its environment.

MODELS AND METHODS

Model of intracellular calcium pathway

A schematic of our model for the dynamics of intracellular calcium oscillations and intercellular calcium diffusion is shown in Fig. 1. The pathway involves primarily the intracellular reaction dynamics and the intercellular diffusion of cytoplasmic calcium and inositol-1,4,5-trisphosphate (IP_3). The intracellular chemical reaction process is based on a model introduced by Politi *et al.* [31]. For the sake of clarity, we describe this model in some detail. The intracellular calcium pathway starts with an extracellular agonist combining with the G-protein-coupled receptors on the cell's membrane to activate phospholipase C (PLC). It is, in turn, able to catalyze the production of IP_3 [32]. IP_3 then can bind to the IP_3 receptor, IP_3R, to open calcium channels in the membrane of the Endoplasmic Reticulum (ER). This process releases stored Ca^{2+} into the cytosol. Meanwhile, the cytoplasmic Ca^{2+} creates both positive and negative feedback conditions in the production of IP_3. For the positive feedback condition, the cytoplasmic Ca^{2+} is capable of activating the PLC isoforms to release more IP_3 [33]. For the negative feedback condition, the increase of cytoplasmic Ca^{2+} can activate the IP_3 degradation via IP_3 3-kinase (IP_3K). Different from other signaling molecules, high levels of intracellular calcium are toxic and cannot be degraded. Cells control the intracellular calcium level by buffering, sequestering in specialized compartments, and expelling to the extracellular space [34, 35].

The intracellular chemical reaction dynamics is formulated into a system of coupled differential equations involving four dynamical variables: the calcium concentration in the cytosol, *c*; the IP_3 concentration in the cytosol, *p*; the calcium concentration in the ER stores, *s*; and the fraction of IP_3R that has not been made inactivate by Ca^{2+}, *r*. The rate equation for the IP_3 concentration takes the following form:

$$\frac{dp}{dt} = f(c,p) = v_{PLC} - v_{\deg} = v_{PLC} - (v_{5P} + v_{3K}) = \left(V_{PLC} \frac{c^2}{K_{PLC}^2 + c^2} \right) - \left(k_{5P} + k_{3K} \frac{c^2}{K_{3K}^2 + c^2} \right) p \ , \qquad (1)$$

where v_{PLC} and $v_{\deg}$ represent the production and degradation rate of IP_3, respectively. V_{PLC} is the maximum production rate of PLC that depends on the agonist concentration. K_{PLC} characterizes the sensitivity of PLC to Ca^{2+}; v_{3K} and v_{5P} are the rates of IP_3 phosphorylation and dephosphorylation, respectively. The phosphorylation rate k_{3k} is described by a Hill function with the half-saturation constant K_{3K} [36]. The rate equation for the cytoplasmic Ca^{2+} is in the following form:

$$\frac{dc}{dt} = g(c,p) = v_{rel} - v_{serca} = \left[k_1 \left(r \frac{c}{K_a + c} \frac{p}{K_p + p} \right)^3 + k_2 \right](s-c) - V_{serca} \frac{c^2}{K_{serca}^2 + c^2} \cdot \quad (2)$$

For the sake of simplicity, the total calcium concentration in the cell, c_{tot}, is conserved and is represented as $c_{tot} = c + \beta s$, where β is the ratio of effective cytoplasmic volume to effective ER volume (both accounting for Ca^{2+} buffering). Therefore, the calcium concentration in the ER store can be expressed as

$$s = \frac{c_{tot} - c}{\beta}. \quad (3)$$

The dynamics of IP_3R inactivation by Ca^{2+} is shown as follow:

$$\frac{dr}{dt} = v_{rec} - v_{inac} = \frac{1}{\tau_r}\left(1 - r\frac{K_i + c}{K_i}\right). \quad (4)$$

In our numerical simulations of the intracellular pathway, we use the model parameters reported by Politi [31]. We limit ourselves to the model supporting calcium positive feedback, in which the phosphorylation rate k_{3k} is set to zero. The corresponding parameters are summarized in Table 1. The numerical solutions of these differential equations are obtained by using the 4th-order Runge-Kutta algorithm with step size, Δt = 0.01 s.

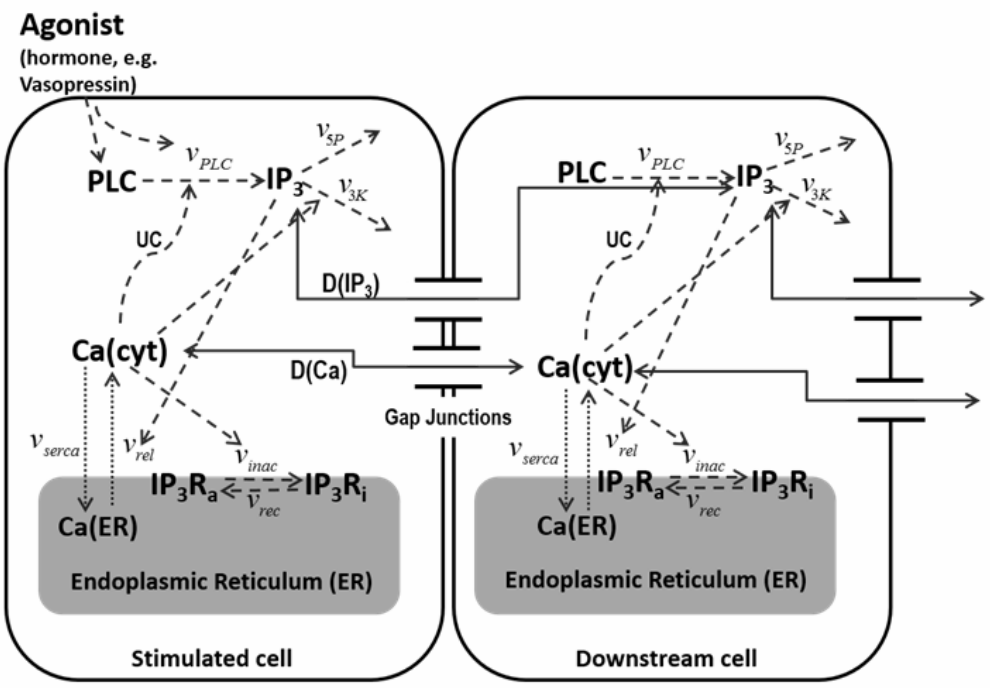

Fig. 1. Reaction/diffusion process of Ca^{2+} and IP_3 metabolism included in the model. The solid, dashed, and dotted arrows indicate molecular diffusion, regulatory interactions, and reaction/transport steps respectively. The bold quantities indicate the following model variables: IP_3, the cytoplasmic IP_3; Ca(*cyt*), the free cytoplasmic Ca^{2+}; Ca(*ER*), the free Ca^{2+} in the ER; IP_3R_a, the active conformation of the IP_3R. The other abbreviations denote IP_3R_i, the inactive conformation of the IP_3R; v_{serca}, the active Ca^{2+} transport into the ER; v_{PLC}, the production rate of IP_3; v_{rel}, the rate of Ca^{2+} release through the IP_3R; v_{inac} and v_{rec}, the rates of Ca^{2+}-induced IP_3R inactivation and recovery, respectively; v_{5P} and v_{3K}, the rates of IP_3 dephosphorylation and phosphorylation, respectively; $D(IP_3)$ and $D(Ca)$, the diffusion coefficient of IP_3 and Ca, respectively; and *UC*, the threshold of Ca needed to activate PLC.

Table 1. Values of reaction/diffusion model parameters.

Parameters	Description	Value
	IP_3 dynamics parameters	
K_{3K}	Half-activation constant of IP_3K	0.4 μM
k_{3K}	IP_3 phosphorylation rate constant	0
k_{5P}	IP_3 dephosphorylation rate constant	0.66 s^{-1}
K_{PLC}	Half-activation constant of PLC	0.2 μM
V_{PLC}	Maximum production rate of IP_3	1.5 μM s^{-1}
	Ca^{2+} transport and structural parameters	
β	Ratio of effective volumes ER/cytosol	0.185
V_{serca}	Maximal SERCA pump rate	0.9 μM s^{-1}
K_{serca}	Half-activation constant	0.1 μM
c_{tot}	Total Ca^{2+} concentration	2 μM
	IP_3R parameters	
k_1	Maximal rate of Ca^{2+} release	1.11 s^{-1}
k_2	Ca^{2+} leak	0.0203 s^{-1}
K_a	Ca^{2+} binding to activating site	0.08 μM
K_i	Ca^{2+} binding to inhibiting site	0.4 μM
K_p	IP_3 binding	0.13 μM
τ_r	Characteristic time IP_3R inactivation	12.5 s
	Reference Diffusion parameters	
D^*_{Ca}	Diffusion coefficient rate of Ca^{2+}	0.005 s^{-1}
D^*_{IP3}	Diffusion coefficient rate of IP_3	$10\, D^*_{Ca}$
UC	Threshold of Ca^{2+} to activate PLC	0.057 μM

We illustrate the oscillatory behavior of the intracellular calcium concentration of individual cell in Fig. 2. Following Politi, we can increase the frequency of the intracellular calcium oscillations by increasing the agonist concentration. For an isolated cell, the frequency of intracellular calcium oscillation does not vary so much at constant V_{PLC} (see Fig. 3). The IP_3 activity follows a similar dynamics.

Fig. 3 illustrates the period of intracellular calcium oscillation generated in an isolated cell with initial calcium concentration, $[Ca]_I = 0.05$ μM. Initially, the period between the oscillating peak #1 and #2 is 1787 time steps. However, the period between the peak #2 and #3 sharply decreases to 1681 time steps (point #2 in Fig. 3), which is followed by a steady state with the period equal to 1672 or 1673 time steps. We have verified that different initial concentrations result in very similar period behavior.

Integration of intracellular calcium pathway into multicellular diffusion model

Politi's model only considers the intracellular dynamics in an isolated cell. To use Politi's model to describe the calcium and IP_3 dynamics in a

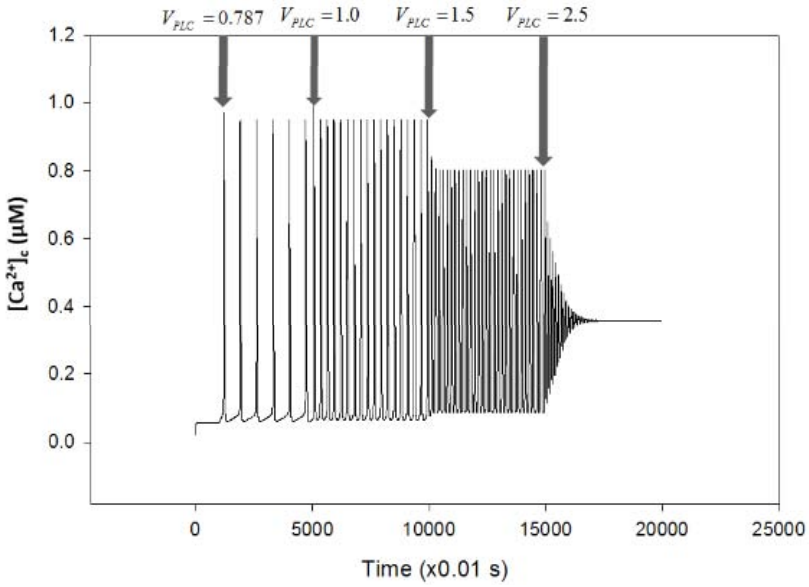

Fig. 2. Politi model: Agonist-induced intracellular calcium oscillation with stepwise increases in the agonist concentration (*arrows*) corresponded by an increase in V_{PLC}. The Y-axis represents the cytosolic calcium concentration with unit "μM". The X-axis represents the time with unit "0.01 s". $V_{PLC} = 0.3$ μM s^{-1} for t < 1000 with successive increases to 0.787, 1.0, 1.5, and 2.5 μM s^{-1}.

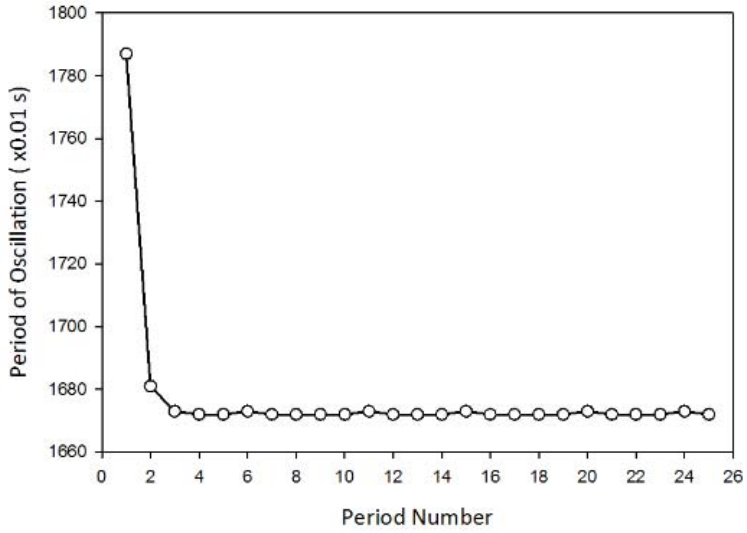

Fig. 3. Period of intracellular calcium oscillation in an isolated cell. The X-axis represents the subsequent maxima. The Y-axis represents the value of time (*in units of 0.01 s*) corresponding to the occurrence of each maximum.

multicellular system, we need to add the phenomenon of diffusion of both Ca^{2+} and IP_3 driven by the concentration gradients between neighboring cells. The multicellular structure considered in this model is composed of a single linear chain of N cells with periodic boundary conditions (PBC). In such a chain, in which every cell is connected to two other cells (diffusion between nearest neighbor cells), one can write the one-dimensional time-dependent reaction/ diffusion equation for Ca^{2+} and IP_3:

$$\frac{\partial c}{\partial t} = D_{Ca}\frac{\partial^2 c}{\partial x^2} + g(c,p) = D^*_{Ca}\left[c(x_{i+1},t_n) - 2c(x_i,t_n) + c(x_{i-1},t_n)\right] + g(c,p), \quad (5)$$

and

$$\frac{\partial p}{\partial t} = D_{IP3}\frac{\partial^2 p}{\partial x^2} + f(c,p) = D^*_{IP3}\left[p(x_{i+1},t_n) - 2p(x_i,t_n) + p(x_{i-1},t_n)\right] + f(c,p), \quad (6)$$

where "D_{Ca}" and "D_{IP3}" are the diffusion coefficients of Ca^{2+} and IP_3. "x" and "t" are the position and time variables. In Eq. (5) and (6), we have discretized the equation in space and time using finite differences. "$t_n = n\Delta t$" refers to the discretized time line with a time step of Δt. $D_{Ca}/\Delta x^2$ and $D_{IP3}/\Delta x^2$ are defined as the diffusion coefficient rate of Ca^{2+} and IP_3 with unit "per second", "s^{-1}", which we denote D^*_{Ca} and D^*_{IP3}, respectively. "Δx" refer to the nearest neighbor intercell-distance. To implement PBC, we impose the cyclic condition on the index "i": cell i+1 = *cell* 1 if I = N and cell i-1 = *cell* N if i=1. The term on the left-hand side is the rate of change of intracellular Ca^{2+}/IP_3 concentration in cell "i". The concentration for the next time increment, n+1, can be calculated from concentration values at the previous time increment, n. We assume that diffusion occurs only between nearest neighboring cells through their membrane via gap junctions. We further assume that the distribution of gap junctions in the plasma membrane is spatially uniform and that the diffusion coefficients are constants independent of cell number. Note that the mobility of Ca^{2+} through gap junction is restricted in comparison to that of IP_3 because of the higher buffering capacity of cytoplasm for Ca^{2+} than for IP_3 [37]. Thus, IP_3 diffuses much faster than Ca^{2+} [38]. For the sake of simplicity, we set $D^*_{IP3} = 10D^*_{Ca}$ in our model.

In combining intracellular dynamics and intercellular diffusion, at a given time, t_{n-1}, for each cell "i", we effectively solve Eq. (1), (2) and (4) by using the 4th order Runge-Kutta method to evolve the c and p concentrations at the time, t_n, due to intracellular dynamics. Meanwhile, the updated $p(x_i,t_n)$ and $c(x_i,t_n)$ are used in the diffusion part of Eq. (5) and (6) to impact the Ca^{2+}/IP_3 concentration in the neighboring cells. We have verified that this algorithm has fully converged for the time step Δt = 0.01 s. For this we have implemented the algorithm for smaller time steps of $\Delta t/2$ and $\Delta t/4$, and verified that one obtains the same reaction/diffusion dynamics.

To study the propagation of trains of calcium waves in a multicellular one-dimensional chain, we initially stimulate a single cell in the center of the chain with the agonist. This cell will be subsequently called: "stimulated cell". PLC of the stimulated cell is activated initially by the extracellular agonist to induce intracellular Ca^{2+}/IP_3 oscillations. All other cells in the chain that are not initially stimulated are referred to as "downstream cells". One may visualize the downstream cells as forming a cellular microenvironment in which the stimulated cell is embedded.

The reaction dynamics of the stimulated cell increases its calcium concentration. Diffusion of Ca^{2+} between the stimulated cell and its neighboring downstream cells elevates the Ca^{2+} concentration in downstream cells. To enable the propagation of a train of calcium waves that is initiated by the oscillation of the stimulated cell, we introduce a threshold based on the calcium concentration for inducing Ca^{2+}/IP_3 positive feedback in downstream cells (Fig. 1). When the cytoplasmic Ca^{2+} concentration reaches a value exceeding a threshold, *UC*, the positive feedback effect of cytoplasmic Ca^{2+} is activated to increase the production rate of IP_3. If the cytoplasmic Ca^{2+} concentration is below the threshold, PLC isoforms are not activated. This enables the synchronized development of collective spatio-temporal response of multicellular architectures. This extension is based not only on diffusion but also on an additional amplification mechanism

through the generation of IP_3 and the Ca^{2+}-dependent activation of PLC [39].

In the simulation, the multicellular chain consists of 301 cells. The central cell (cell 151) is the stimulated cell. The size of the chain is chosen such that the calcium trains of waves never reach the ends of the chain (cells 1 and 301) during the time of the simulation. So even though we have implemented PBC, these conditions are never required during the simulation time reported here. The initial concentrations of Ca^{2+} and IP_3 are set to 0.05 μM. The continuous presence of agonist is required to evoke the sustained intercellular calcium waves [40]. Therefore, the V_{PLC} of the stimulated cell is kept at 1.5 μM s^{-1}. All other cells have their initial V_{PLC} set to 0.01 μM s^{-1} which is too low to activate the intracellular calcium oscillation. When the calcium concentration exceeds UC for the first time in a downstream cell, its V_{PLC} is set to 1.5 μM s^{-1} for the remaining time of the simulation. The parameters of the diffusion model are listed in Table 1 with those parameterizing the intracellular reaction dynamics.

RESULTS AND DISCUSSION

A comparison between the calcium oscillation of the stimulated cell and its first neighboring downstream cell is shown in Fig. 4. Because the diffusion process is symmetric, we just show the temporal evolution of the calcium concentration on one side of the chain. The IP_3 activity shows a similar dynamic.

Initially, only the stimulated cell is triggered to generate calcium oscillation. Meanwhile, cytosolic calcium diffuses from the stimulated cell to the downstream cells through gap junctions. Once the calcium concentration in the downstream cells rises to a level exceeding the threshold "*UC*", the PLC in the downstream cells is activated. That is, we set $V_{PLC}^{sc} = V_{PLC}^{dc} = 1.5$ μM s^{-1}, where the superscripts "sc" and "dc" denote "stimulated cell" and "downstream cells", respectively. This process sustains the propagation of a calcium wave. In Fig. 4, the cytosolic calcium oscillation frequency of both the stimulated cell and the 1st neighboring cell is nearly the same. However, a slight phase shift

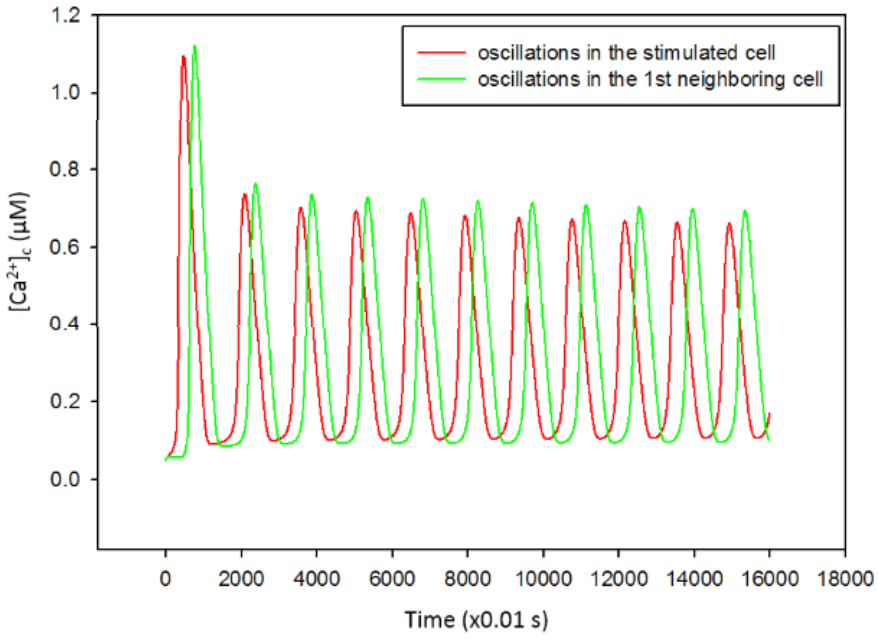

Fig. 4. Calcium oscillation based on reference parameters in stimulated cell and its first neighboring cell. The Y-axis represents the cytosolic calcium concentration with unit "μM". The X-axis represents the time unit "0.01 s". The red line stands for the intracellular calcium oscillation in the stimulated cell. The green line shows the intracellular calcium oscillation in the 1st neighboring cell.

occurs in the 1st neighboring cell because of a time lag imposed by the Ca^{2+}/IP_3 diffusion process. This latency is inversely proportional to the value of the diffusion coefficients. The IP_3 activity shows similar dynamics.

We now turn to a description of the propagation of calcium train of waves resulting from the coupled reaction/diffusion model (see Fig. 5).

Fig. 5 illustrates the temporal and spatial evolution of the train of calcium waves produced by the multicellular reaction/diffusion model. Initially, intracellular calcium oscillation is induced by the extracellular agonist in the central cell (cell 151). At the time step (T) T = 474 (in units of 0.01s), the first calcium pulse in the central cell, which is marked by a star, "★", reaches its highest value (Fig. 5 A). As time marches, this pulse splits into two pulses, propagating in opposite directions from the stimulated cell. Because pulse propagation is symmetrical about the center of the chain, we number the pulses from the pulse at the front of the train on the left side of the stimulated cell, only. The pulse labeled with a "star" corresponds to the 1st pulse, or say pulse #1 in the train. As time proceeds, the central cell undergoes subsequent oscillations. These oscillations emit calcium pulses that propagate in opposite directions along the chain. This process leads to the formation of the two opposite intercellular calcium wave trains (ICWTs). The wavelength of the ICWTs (separation distance between adjacent pulses) will be quantified by the number of cells between two maxima. It takes a value between 4 and 5 cells. After the 7th oscillation of the stimulated cell, at T = 9373, pulse #1 is located on cell 119. The 7th calcium pulse supported by the central cell reaches its highest level when the 6th pulse reaches cell 147 (Fig. 5 B). The interval between these two pulses now corresponds to a segment containing 3 cells (involving cells 148, 149, 150). This is the beginning of the spontaneous heterogenization of the train of pulses propagating along the chain of cells, that is a time-dependent decrease in the wavelength of the train of pulses at T = 14943, when the calcium concentration in the central cell reaches its 11th maximum, the train of pulses is composed of two distinct regions. A train of pulses with a 4- to 5-cell wavelength (between pulses 1 and 9) and a central region with three pulses (#9 to #11) separated by segments containing 3 cells (Fig. 5 C). At T = 21709, the central region of the chain becomes even more heterogeneous as a wavelength of 2-cell interval appears between pulses #15 and #14 (Fig. 5 D) in addition to the existing 3-cell interval wavelengths already described. For T = 27043, the central region is composed of five pulses with 2-cell and 3-cell wavelengths (Fig. 5 E). Finally, the train of pulse is fully heterogenized with 4- to 5-cell distances separating the pulses #1 to #21, and a central region composed of pulses #21 through #26 separated by 3-, 2- and 1-cell wavelength. The wavelength of the train of waves decreases as one approaches the stimulated cell from the front pulse (Fig. 5 F). Although we only reported calcium concentration in Fig. 5, the concentration of IP_3 follows a very similar dynamics.

Fig. 6 illustrates the downward tendency of the period of intracellular calcium oscillation generated in the stimulated cell. Similar to Fig. 3, the period of oscillation shown in Fig. 6 begins with a sharp decrease followed by a slow reduction before reaching a constant value. The initial rapid decrease is similar to that observed for the isolated cell in Fig. 3. This is representative of the dynamics of the intracellular pathway. However, the slow varying region of Fig. 6 contains 21 points (point #2 to #22, i.e. 21 periods) instead of 2 points (point #2 and #3) as was shown in Fig. 3. Moreover, the period of oscillation at steady state in Fig. 6 is smaller than that in Fig. 3. We observe two effects, these being: (a) a slow rate of evolution towards steady state in the multicellular structure compared to the isolated cell, and (b) a steady state period of oscillation that depends on the cell environments indicate that the intracellular dynamics is probably controlled by the diffusion process.

The calcium diffusion process is bi-directional and is driven by the calcium concentration gradient between the neighboring cells. We name the diffusion from the center of the chain to the edges of the chain "forward diffusion" and the diffusion from the edges to the center "retrograde diffusion". When the calcium pulses in the central cell split into two pulses that subsequently propagate outward, the calcium concentration of the central cell decreases to form a trough while the calcium concentration of the downstream cells remains high. Thus, a calcium concentration gradient is established between

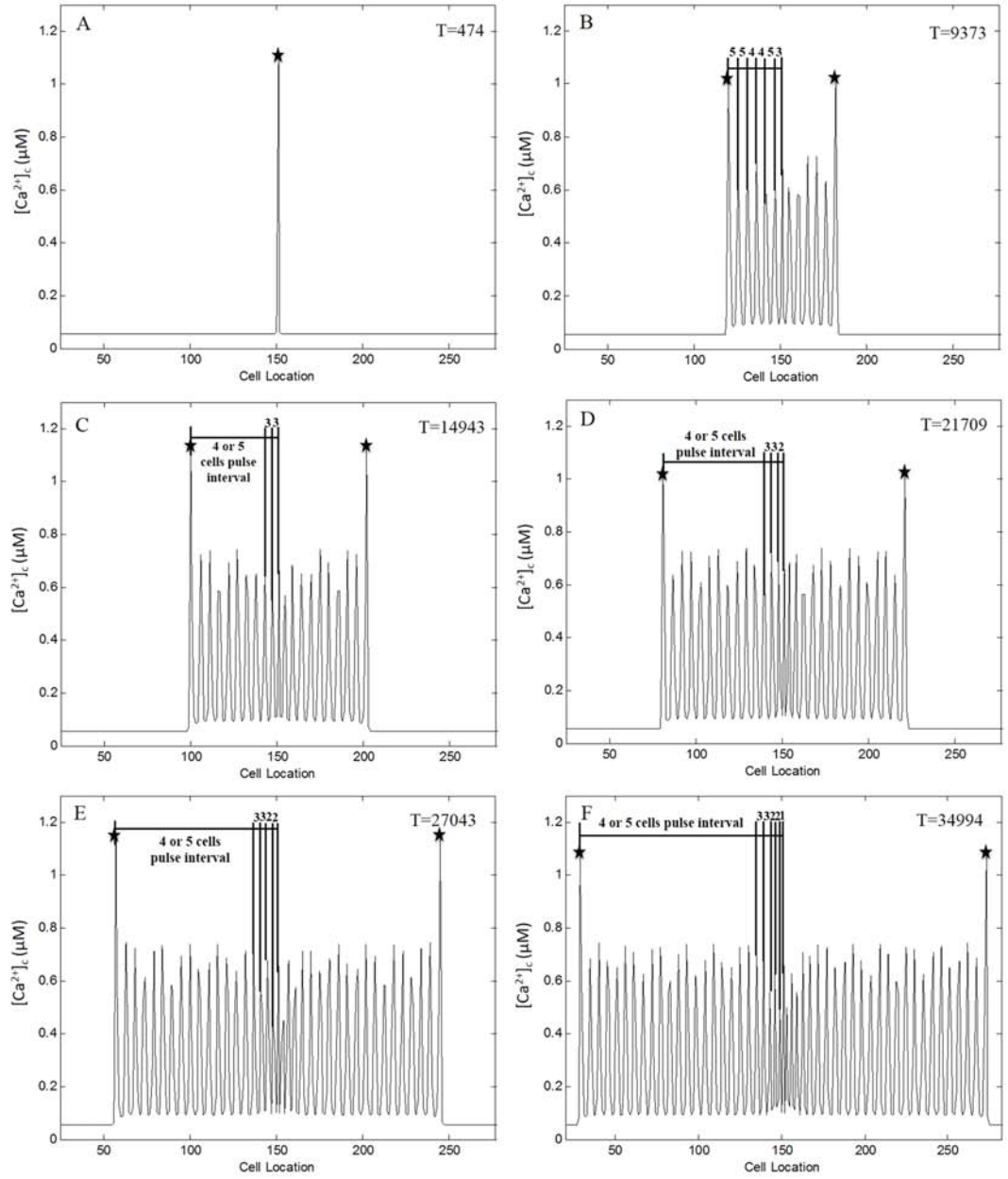

Fig. 5. Snapshots of the propagating train of waves along the chain of cells. The snapshots are reported at different times expressed in units of "0.01 s". The Y-axis represents the cytosolic calcium concentration. The X-axis represents the location of cells. Cell 151 is the stimulated cell. (A) Train of pulses at time point T = 474; the front of the train of pulse is marked by a star, "★". In subsequent snapshots, the front of the signal train is also marked by a star. (B) Train of pulses at time point T = 9373; the separation distance between pulses (wavelength of the train) amounts to a segment of the chain containing 4 to 5 cells for the first 6 pulses. This wavelength reduces to a segment containing 3 cells between pulse #7 and #6. (C) Train of pulses at time point T = 14943; the train of pulses keeps propagating and retains a wavelength of 4 to 5 cell segments between pulses #1 through #9. The wavelength amount to a 3 cell segment between pulses #9 and #10, #10 and #11. (D) Train of pulses at time point T = 21709; the central area with short wavelength expands spatially; the pulse interval between the newest calcium pulse generated by the central cell and the adjacent pulse decreases to a 2-cell segment. (E) Train of pulses at time point T = 27043; the central region with decreasing wavelength keeps expanding. (F) Train of pulses at time point T = 34994; short wavelength region expands further and the wavelength shortens to 1-cell interval.

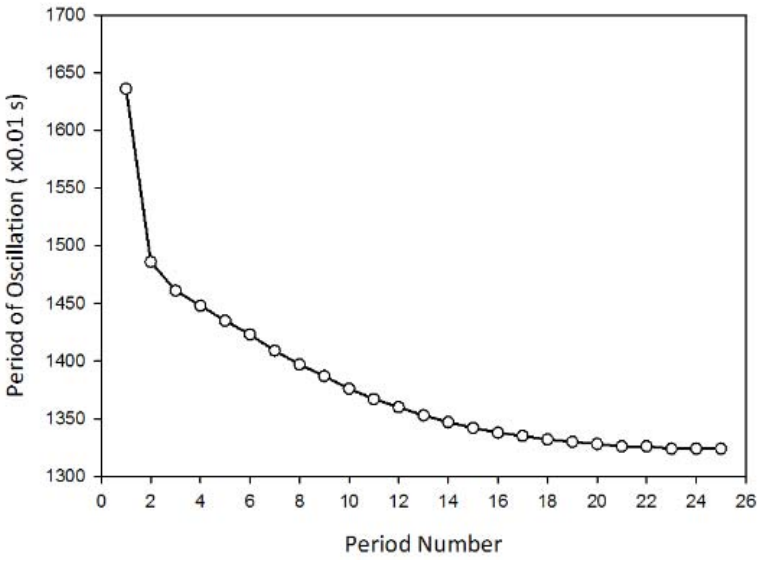

Fig. 6. Period of intracellular calcium oscillation in the central cell. The X-axis represents the subsequent maxima. The Y-axis represents the value of time (*in units of 0.01 s*) corresponding to the occurrence of each maximum.

some of the downstream cells with high calcium concentration and the cells in the vicinity of the central cell with low calcium concentration. Retrograde diffusion will occur, increasing slightly the Ca^{2+} concentration in the central region of the chain. The central cell may, therefore, take less time to reach its highest calcium level. With an increase in the number of calcium pulses along the cell chain, the influence of Ca^{2+} accumulation by retrograde diffusion around the central cell is hypothesized to affect the frequency of its intracellular calcium oscillations.

In order to explain the mechanism of the retrograde diffusion effect, we introduce the concept of an "effective diffusion coefficient". According to Fick's first law, the flux of Ca^{2+} between two neighboring cells is

$$J = -D_{in}\frac{C_n - C_{n+1}}{\Delta x}, \tag{7}$$

where J is the flux of Ca^{2+}; C_n is the calcium concentration of cell n; C_{n+1} is the calcium concentration of cell n+1; D_{in} is the intrinsic diffusion coefficient which is also called the diffusion coefficient in the simulation; and Δx is the intercell spacing. We assume $C_n > C_{n+1}$.

During the propagation process of ICWTs, retrograde diffusion increases C_{n+1} to C_{n+1}^*. We can write the Ca^{2+} flux between cell n and cell n+1 in two ways

$$J = -D_{in}\frac{C_n - C_{n+1}^*}{\Delta x} = -D_{eff}\frac{C_n - C_{n+1}}{\Delta x}, \tag{8}$$

where D_{eff} is an effective diffusion coefficient. Because C_{n+1} is less than C_{n+1}^*, D_{in} should be larger than D_{eff}. In the early stages of the propagation of the train of calcium waves (the first 5 pulses), we assume that the retrograde diffusion effect is not large enough to change the oscillation frequency of the stimulated cell. Therefore, the intrinsic diffusion coefficient, D_{in}, can be used as a surrogate for the effective diffusion coefficient when considering the early stages of propagation of calcium waves.

Fig. 7 illustrates the properties of ICWTs at the early stage of simulations for different effective (intrinsic) diffusion coefficient rates. Fig. 7 E shows the variation of oscillation period of the stimulated cell for different values of the diffusion coefficient. When $D_{in}^*(Ca)$ is less than 0.0017 s^{-1}, there is no intercellular calcium propagation along

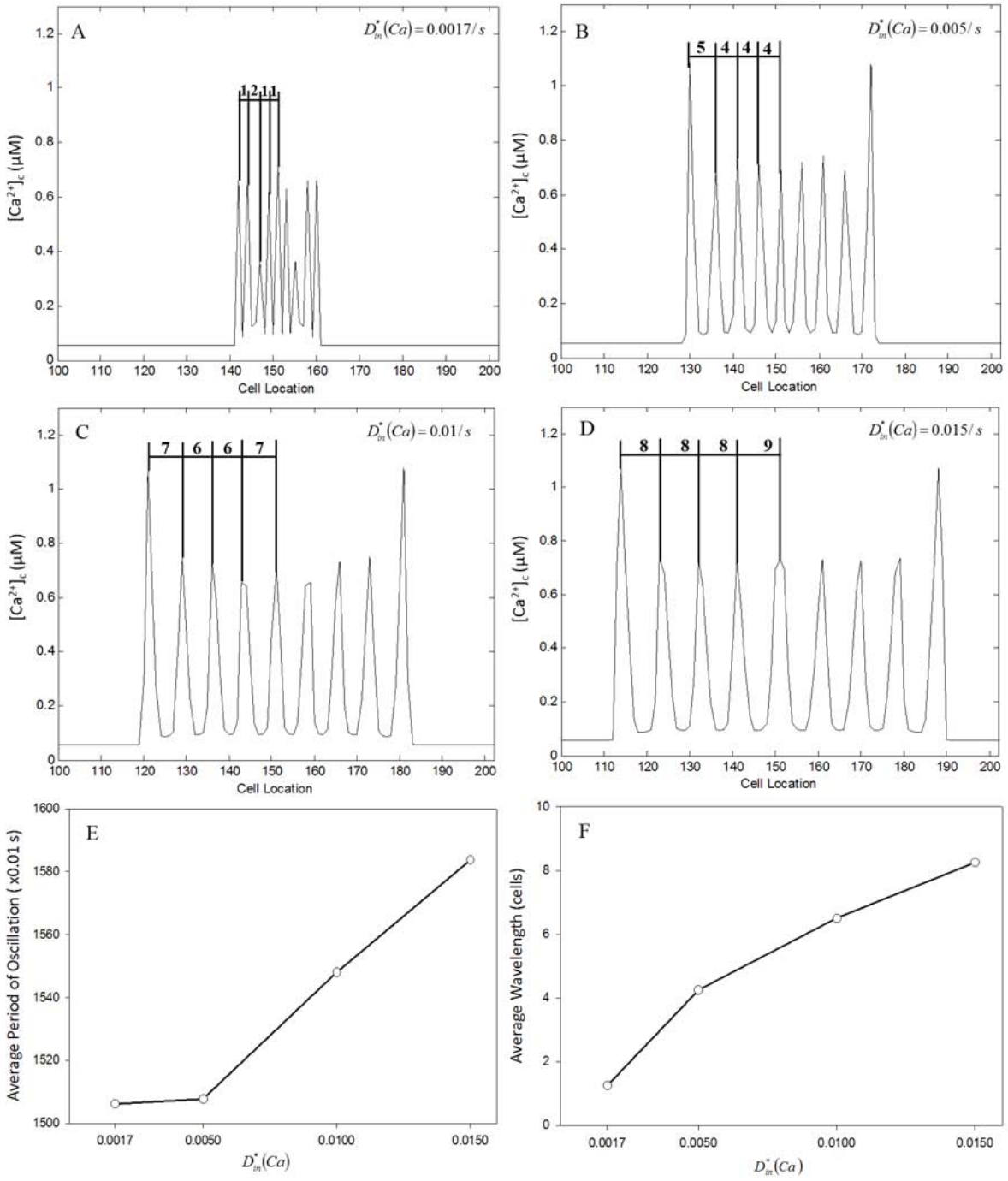

Fig. 7. The properties of ICWTs for different intrinsic calcium diffusion coefficients in the early stage of the ICWTs. (A-D) Early stages of ICWTs for $D^*_{in}(Ca)$ = 0.0017, 0.005, 0.01, and 0.015 s^{-1}, respectively. The Y-axis represents cytosolic calcium concentrations. The X-axis represents cell locations. (E) The average period of intracellular calcium oscillation of the early stages when $D^*_{in}(Ca)$ = 0.0017, 0.005, 0.01 and 0.015 s^{-1}, which are represented by the white dots. The Y-axis represents the average period of oscillation. The X-axis represents the intrinsic diffusion coefficient rate of Ca. (F) The average pulse intervals of the early stages when $D^*_{in}(Ca)$ = 0.0017, 0.005, 0.01 and 0.015 s^{-1}. The Y-axis represents the average pulse intervals. The X-axis represents the intrinsic diffusion coefficient rate of Ca.

the chain. Focusing on $D_{in}^{*}(Ca) \geq 0.0017$ s^{-1}, when $D_{in}^{*}(Ca)$ is equal to or larger than 0.0017 s^{-1}, the average period of oscillation increases with increasing diffusion coefficient. Fig. 7 F illustrates the relationship between the effective diffusion coefficient and the average wavelength. This figure shows that the wavelength decreases with a decreasing diffusion coefficient, at least in the early stages of the propagation. This observation can be used to shed light on the decreasing wavelength we reported during the later stage of propagation. Over time the retrograde diffusion process effectively reduces the diffusion flux in the vicinity of the stimulated cell and therefore leads to a reduced effective diffusion coefficient. An effective diffusion coefficient with a value smaller than that of the intrinsic coefficient would result in a shortening of the wavelength.

CONCLUSION

This modeling and simulation study of calcium oscillations and trains of calcium waves in a chain-like cell network shows that the dynamics of cells embedded in a network is significantly different from that of an isolated cell. In particular we have demonstrated that the transient and steady state frequency of calcium oscillations of a cell stimulated with an agonist depends on its microenvironment, in this case, cell neighbors. This effect is attributed to a crosstalk between the stimulated cell and its environment through retrograde diffusion of calcium and IP_3. As a growing number of cells in the chain are excited over time and undergo oscillations, retrograde diffusion arising from an expanding train of pulses affects the calcium and IP_3 fluxes in the region that originated the train of waves, that is, in the vicinity of the original stimulated cell. The neighborhood of the stimulated cell forms a "signaling niche" that acts on the stimulated cell itself and affects its dynamics. After stimulation of the single cell, the cellular niche responds to its Ca^{2+} and IP_3 oscillations and signals back through gap-junction mediated diffusion thereby influencing the calcium behavior in the originating cell. This crosstalk leads to a dynamical regulation of the stimulated cell's oscillation frequency. Given the importance in intracellular calcium dynamics in cell function, the niche-dependent changes will likely influence subsequent functions of that single cell. Our simulations always involved the activity of the same, single originating cell and the subsequent impact on calcium behavior throughout the network.

In the tissue space, there will be multiple "originating cells" (meaning more than one cell in the interconnected system is receiving an external activating signal within the same time period), all of which comprise the cellular neighborhood. Thus, the originating cell in one instance is also a potential modifier cell to a neighborhood cell that is originating an oscillation. So, any given cell within a cell neighborhood is both an originating cell and a modifier cell to signals generated elsewhere within the neighborhood. Therefore, the activity of the cell system is greater than the sum of its parts because this type of calcium wave regulation is occurring across the entire system as multiple different cells originate calcium oscillations. Key to this conceptual model is a single-cell centric perspective whereby each cell acts as a signal originating cell while also populating the cellular niche of other cells within the network. Even though we focused on one originating cell in this study, it should be possible to adapt the computational model to examine more complex paradigm.

This observation may have striking implications on the role of calcium signaling on cross-level interdependence in multicellular architectures in terms of signal generation and decoding. We have shown that the environment-dependent cross-talk results in Ca^{2+} and IP_3 regulation as well as control over oscillation frequency. Decoding of structural information by individual cells would subsequently need cellular control on frequency dependent intracellular pathways such as frequency-dependent protein phosphorylation by a Ca^{2+}-calmodulin activated kinase which was shown to be ubiquitous in a wide variety of cell types [41]. Therefore, it seems more likely that our calcium-based environment dependent frequency-encoding mechanism is operative in a range of multicellular architectures and tissues.

ACKNOWLEDGEMENT

This work is supported by the James S. McDonnell Foundation 21st Century Science Initiative in

Studying Complex Systems and NIH Director's New Innovator Award (1DP2OD007161-01). I thank the Natural Science Foundation of Jiangxi Province of China for sponsoring the publication of this article.

CONFLICT OF INTEREST STATEMENT

There are no conflicts of interest.

REFERENCES

1. Bissell, M. J., Rizki, A. and Mian, I. S. 2003, Current Opinions in Cell Biology, 15, 753-762.
2. Hansen, R. K. and Bissell, M. J. 2000, Endocrine-Related Cancer, 7, 95-113.
3. Nelson, C. M. and Bissell, M. J. 2006, Annu. Rev. Cell. Dev. Biol., 22, 287-309.
4. Heng, H. H. Q. 2007, BioEssays, 29, 783-794.
5. Barcellos-Hoff, M. H. 2001, J. Mammary Gland Biology and Neoplasia, 6, 213-221.
6. Kirshner, J., Chen, C. J., Liu, P., Huang, J. and Shively, J. E. 2003, Proc. Natl. Acad. Sci. USA, 100, 521-526.
7. Davidson, L. A. 2008, Current Topics in Developmental Biology, 81, 113-133.
8. Mikos, A. G., Herring, S. W., Ochareon, P., Elisseeff, J., Lu, H. H., Kandel, R., Schoen, F. J., Toner, M., Mooney, D., Atala, A., Van Dyke, M. E., Kaplan, D. and Vunjak-Novakovic, G. 2006, Tissue Engineering, 12, 3307-3340.
9. Ketchedjian, A., Jones, A. L., Krueger, P., Robinson, E., Croutch, K., Wolfinbarger, L. and Hopkins, R. 2005, Ann. Thorac. Surg., 79, 888-896.
10. Lacar, B., Young, S. Z., Platel, J. C. and Bordey, A. 2011, Eur. J. Neurosci., 34, 1895.
11. Dani, J. W., Chernjavsky, A. and Smith, S. J. 1992, Neuron, 8, 429-40.
12. Watts, D. J. and Strogatz, S. 1998, Nature, 393, 440-442.
13. Malmersjo, S., Rebellato, P., Smedler, E., Planert, H., Kanatani, S., Liste, I., Nanou, E., Sunner, H., Abdelhady, S., Zhang, S., Andang, M., Manira, A., Silbergerg, G., Arenas, E. and Uhlen, P. 2013, PNAS, 110, E1524.
14. Othmer, H. G. and Scriven, L. E. 1971, J. Theor. Biol., 32, 507-537.
15. Turing, A. M. 1952, Philosophical Transactions of the Royal Society of London, Series B, Biological Sciences, 237, 37-72.
16. Eray, M., Deymier, P. A., Hoying, J. B., Runge, K. and Vasseur, J. O. 2008, Physica D, 237, 2777-2786.
17. Deymier, P. A., Eray, M., Deymier, M. J., Runge, K, Hoying, J. B. and Vasseur, J. O. 2010, Phys. Rev. E., 81, 041915.
18. Dobrzynski, L. and Puszkarski, H. 1989, Journal of Physics: Condensed Matter, 1, 1239-1245.
19. Tran, Q. K., Ohashi, K. and Watanabe, H. 2000, Cardiovascular Research, 48, 13-22.
20. Deymier, P. A., Runge, K., Deymier, M. J., Hoying, J. B. and Vasseur, J. O. 2010, Phys. Rev. E., 82, 041913.
21. Long, J., Junkin, M., Wong, P. K., Hoying, J. B. and Deymier, P. A. 2012, PLoS Comput. Bio., 8, e1002847.
22. Bellinger, S. 2005, Neurocomputing, 65-66, 843-850.
23. Edwards, J. R. and Gibson, W. G. 2010, J. Theor. Biol., 263, 45-58.
24. Goldberg, M., De Pitta, M., Volman, V., Berry, H. and Ben-Jacob, E. 2010, PLoS Comput. Bio., 6, e1000909.
25. Meyer, T. and Stryer, L. 1988, Proc. Natl. Acad. Sci., 85, 5051-505.
26. Hofer, T., Venance, L. and Giaume, C. 2002, The Journal of Neuroscience, 22, 4850-4859.
27. Berridge, M. J. 1991, Cell Calcium, 12, 63-72.
28. Goldbeter, A., Dupont, G. and Berridge, M. J. 1990, Proc. Natl. Acad. Sci., 87, 1461-1465.
29. Gracheva, M. E. and Gunton, J. D. 2003, J. Theor. Biol., 221, 513-518.
30. Rooney, T., Sass, E. and Thomas, A. P. 1989, J. Biol. Chem., 264, 17131-17414.
31. Politi, A., Gaspers, L. D., Thomas, A. P. and Hofer, T. 2006, Biophysical Journal, 90, 3120-3133.
32. Rhee, S. G. 2001, Annu. Rev. Biochem., 70, 281-312.
33. Harootunian, A. T., Kao, J. P., Parajape, S. and Tsien, R. Y. 1991, Science, 251, 75-78.
34. Combettes, G. L. and Leybaert, L. 2007, Int. Rev. Cytol., 261, 193-245.

35. Verkhratsky, A., Orkand, R. K. and Kettenmann, H. 1998, Physiol. Rev., 78, 99-141.
36. Communi, D., Vanweyenberg, V. and Erneux, C. 1997, EMBO J., 16, 1943-1952.
37. Sanderson, M. J., Charles, A. C., Boitano, S. and Dirksen, E. R. 1994, Molecular and Cellular Endocrinology, 98, 173-187.
38. Allbritton, N. L., Meyer, T. and Stryer, L. 1992, Science, 258, 1812-1815.
39. Berridge, M. J. 1993, Nature, 361, 315-325.
40. Gaspers, L. D. and Thomas, A. P. 2005, Cell Calcium, 38, 329-342.
41. Koninck, P. De. and Schulman, H. 1998, Science, 279, 227.